arXiv:1609.08041v1 [physics.optics] 26 Sep 2016

From the generalized reflection law to the realization of perfect anomalous reflectors

A. Díaz-Rubio[1], V. S. Asadchy[1,2], A. Elsakka[1], and S. A. Tretyakov[1]

[1]*Department of Radio Science and Engineering,*

Aalto University, P. O. Box 13000, FI-00076 Aalto, Finland

[2]*Department of General Physics, Francisk Skorina*

Gomel State University, 246019 Gomel, Belarus

Abstract

The use of the generalized Snell's law opens wide possibilities for the manipulation of transmitted and reflected wavefronts. However, known structures designed to shape reflection wave fronts suffer from significant parasitic reflections in undesired directions: In fact, the desired field distributions do not satisfy Maxwell's equations if the boundary conditions are specified in accordance with the generalized Snell's law. In this work, we explore the limitations of the existing solutions for the design of passive planar reflectors and demonstrate that strongly non-local response is required for perfect performance. Ideal reflective surfaces capable of steering the energy into any desired direction have to localize and carry energy along the inhomogeneous reflective surface. A new paradigm for the design of perfect reflectors based on energy surface channeling is introduced. We realize and experimentally verify a theoretically perfect design of an anomalously reflective surface using an array of rectangular metal patches backed by a metallic plate. This conceptually new mechanism for wavefront manipulation allows the design of thin perfect reflectors, offering a versatile design method applicable to other scenarios such as focusing reflectors or surface wave manipulations, extendible to other frequencies.

I. INTRODUCTION

The classical approach to the design of wave-shaping reflectors for light or microwave radiation is based on the geometrical optics. A flat mirror obviously obeys the usual reflection law: in the absence of dissipation, all reflected rays go into the specular direction without changing the field amplitude. The distribution of reflected field intensity can be engineered by shaping the reflecting surface. Due to the differences of the ray-propagation path lengths, the phase distribution at the reflector aperture can be tuned so that, for example, all rays converge at a point, forming a focal spot. Generalizing the phased-array antenna principle, the same function can be realized in a planar reflector, if the reflection phase is made non-uniform over the reflector surface. In antenna applications, such non-uniform reflectors are called reflectarrays and are usually realized as arrays of resonant antennas [1]. Most commonly, patch antennas are used and the reflection phase from every element is tuned either by reactive loads or by varying patch size or shape. Reflectarrays with subwavelength distances between the array elements are called high-impedance surfaces [2, 3] or metasurfaces [4].

According to the phased-array principle, to reflect an incident plane wave (the incidence angle θ_i) into another plane wave, breaking the usual reflection law (the reflection angle $\theta_\mathrm{r} \neq \theta_\mathrm{i}$), the reflection phase should linearly depend on the corresponding coordinate along the reflector plane. In this situation one can expect that reflections from all the points interfere constructively in a plane wave propagating in the desired direction. Recently, this simple design principle was formulated in form of the "generalized Snell's law" [5]. To understand this law, let us assume that a plane wave is incident at a planar reflecting surface at the incidence angle θ_i and introduce a Cartesian coordinate system with the x-axis along the projection of the wavevector to the reflector plane. If the reflected plane wave is propagating at the reflection angle θ_r and its amplitude is the same as in the incident wave, then the ratio of the tangential electric fields in the reflected wave and in the incident wave at the reflector surface is given by $\exp(j\Phi_\mathrm{r}) = \exp[j(\sin\theta_\mathrm{i} - \sin\theta_\mathrm{r})k_1 x]$. Here, $k_1 = \omega\sqrt{\mu\varepsilon}$ is the wavenumber in the background isotropic medium, and we assume the time-harmonic dependency $e^{j\omega t}$. Obviously, there is a relation between the reflection angle and the gradient of the reflection phase profile

$$\sin\theta_\mathrm{i} - \sin\theta_\mathrm{r} = \frac{1}{k_1}\frac{d\Phi(x)}{dx}, lgrl \tag{1}$$

which is called the generalized reflection law [5].

This design approach has been used to realize various metasurfaces for reflection control, for example, in [6–13], as well as in all known designs of reflectarrays [1]. However, it is easy to see that this simplistic method does not allow one to exactly realize the desired performance: some part of the incident energy is inevitable scattered in non-desired directions (parasitic specular reflection, etc.) or absorbed in the reflector [14, 15]. Parasitic reflections or absorptions are inevitable within this scenario because the boundary conditions on the lossless surface which has the reflection phase as dictated by ǧrl are not satisfied by the desired field distribution. Thus, in all known realizations the power efficiency defined as the ratio of the power sent into the desired direction and the incident power is typically quite low and it decreases when the desired reflection angle deviates more and more from the specular reflection angle. Very recently, it was shown that it is in principle possible to realize anomalously reflecting metasurfaces which operate perfectly, that is, without any parasitic reflections and scattering [14, 16]. Such perfect anomalous reflectors must be either active or realize non-local reflections, that is, the incident energy is not immediately reflected at the incident point, but it is first transported along the surface at some distance [14]. In paper [16], an alternative theoretical approach was introduced (based on interference with additional evanescent waves) and a conceptual design based on three parallel inhomogeneous reactive sheets has been proposed, but no actual realizations are known, to the best of our knowledge.

Inspired by the physical principle of leaky-wave antennas, we demonstrate that a perfect anomalous reflector can be realized as a simple metal pattern on a thin grounded dielectric slab. In this scenario, engineered modulations of the surface reactance ensure the required non-local reflections, which are eventually perfectly launched only in the desired direction. Based on the developed theory we design, manufacture, and experimentally study an example metareflector which reflects a normally incident plane wave into a plane wave at the tilt angle $\theta_{\rm r} = 70^\circ$. The experimental results confirm that this first prototype of metasurfaces for perfect control of reflections operates according to expectations: the realized power efficiency is close to 100%, limited only by dissipation in the metal patches and the dielectric substrate. Parasitic reflections into the specular direction and other directions are seen to be negligible. The proposed simple topology allows cheap mass-production manufacturing based on the conventional printed circuit board technology (microwave frequencies) or

various lithography techniques (terahertz and beyond).

II. THEORY: LOCAL AND NON-LOCAL METAREFLECTORS

A. Conventional design using the generalized reflection law

Metasurfaces for anomalous reflection based on the known generalized reflection law ǧrl are designed for ensuring at every point of the surface a phase shift in reflection according to

$$\Phi_{\mathrm{r}}(x) = (\sin\theta_{\mathrm{i}} - \sin\theta_{\mathrm{r}})k_1 x, \tag{2}$$

with θ_{i} and θ_{r} being the incidence and reflection angles, respectively, while the amplitude of the reflection coefficient is unity (neglecting dissipation losses). The local reflection coefficient defines a periodically modulated boundary surface with the surface impedance $Z_{\mathrm{s}}(x)$. The relation between the reflection coefficient and the surface impedance can be written as

$$\Gamma = \frac{Z_{\mathrm{s}}(x) - \eta_1}{Z_{\mathrm{s}}(x) + \eta_1} = e^{j\Phi_{\mathrm{r}}(x)}, \tag{3}$$

where η_1 is the wave impedance of the background medium. Considering lossless implementations, the surface impedance is purely imaginary and using (2) can be expressed as

$$Z_{\mathrm{s}}(x) = j\frac{\eta_1}{\cos\theta_{\mathrm{i}}}\cot[\Phi_{\mathrm{r}}(x)/2]. \tag{4}$$

Equation (4) is a well-known solution that has been used in numerous works. Examples of reflective metasurfaces designed following this approach can be found in papers [6–13]. Nevertheless, the sum of the incident and one reflected plane wave is not a valid solution for the Maxwell equations with the surface impedance given by (4). This means that when we illuminate a metasurface characterized by the surface impedance given by the generalized reflection law (4) with a plane wave at θ_{i}, in addition to the desired anomalously reflected plane wave at θ_{r}, more plane waves will be exited in the system in order to satisfy the power conservation and the boundary conditions, leading to parasitic reflections.

Let us look into this important feature in more detail. The period of the metasurface D_{x} is defined by requiring that the reflection phase is 2π-periodic: $\Phi_{\mathrm{r}}(x) = \Phi_{\mathrm{r}}(x + D_{\mathrm{x}}) + 2\pi$, and using (2) it can be expressed as

$$D_{\mathrm{x}} = \lambda/|\sin\theta_{\mathrm{r}} - \sin\theta_{\mathrm{i}}|, \tag{5}$$

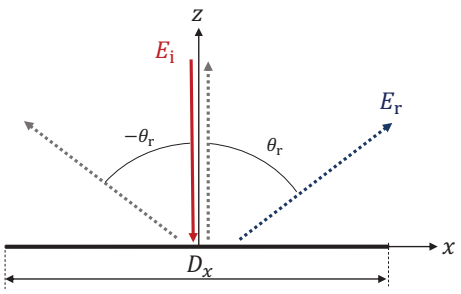

FIG. 1: Propagating waves in the system when $\theta_i = 0°$ and $\theta_r > 30°$

where $\lambda = 2\pi/k_1$ is the wavelength. The period will define the directions where the reflected energy can flow. For example, considering normal incidence, $\theta_i = 0°$, and $\theta_r > 30°$, the energy only can be reflected as plane waves in three different directions (see Fig. 1): the specular direction (θ_i), the desired direction (θ_r) and the symmetric direction ($-\theta_r$). Numerical simulations have been done (using the HFSS package) modeling a metasurface with the impedance boundary described by Eq. (4). Particularly, the impedance boundary has been designed for reflecting the energy from $\theta_i = 0°$ into $\theta_r = 70°$ at the frequency $f = 8$ GHz. Figure 2(a) shows the distribution of the real part of the scattered electric field, where we see an interference pattern produced by these three plane waves. As previously stated, the energy is distributed into three directions producing a modulation of the real part of the Poynting vector, as it is shown in Fig. 2(b). It is important to notice that the amplitude of the reflected wave in the desired direction $E_r = 1.5$ V/m is higher than the incident amplitude $E_i = 1$ V/m, so the metasurface is adding not only a linear phase shift as it is expected from Eq. (3), but also changes the amplitude. This property agrees with the conclusion that more than two propagating plane waves must exist in the system. The efficiency of the design is $\eta = P_r/P_i = 0.757$ and the residuary energy is sent to the other directions. In this definition of the power efficiency η, P_r and P_i are the amplitudes of the Poynting vector of the plane wave reflected in the desired direction and that of the incident plane wave, respectively.

B. Lossy design

Parasitic reflections can be suppressed by allowing power absorption in the metasurface. As is shown in [14, 15], a solution for the Maxwell equations where $E_r = E_i$ can be found

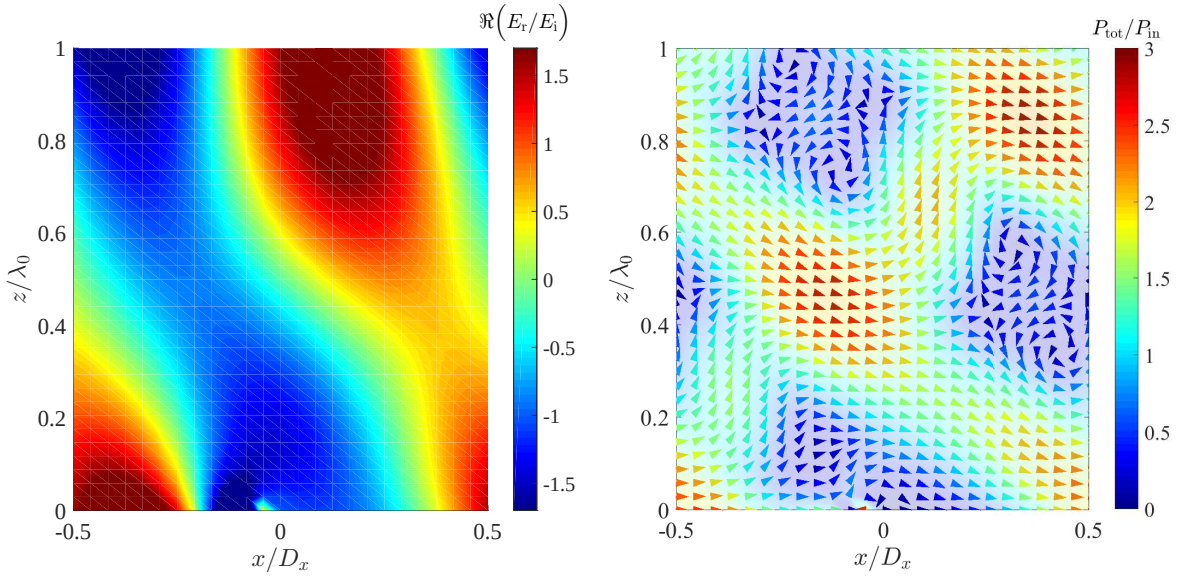

(a) (b)

FIG. 2: Conventional design of a reflector based on the generalized reflection law when $\theta_i = 0°$, $\theta_i = 70°$, $E_i = 1$ V/m and $f = 8$ GHz. (a) Real part of the scattered electric field. (b) Total power density distribution.

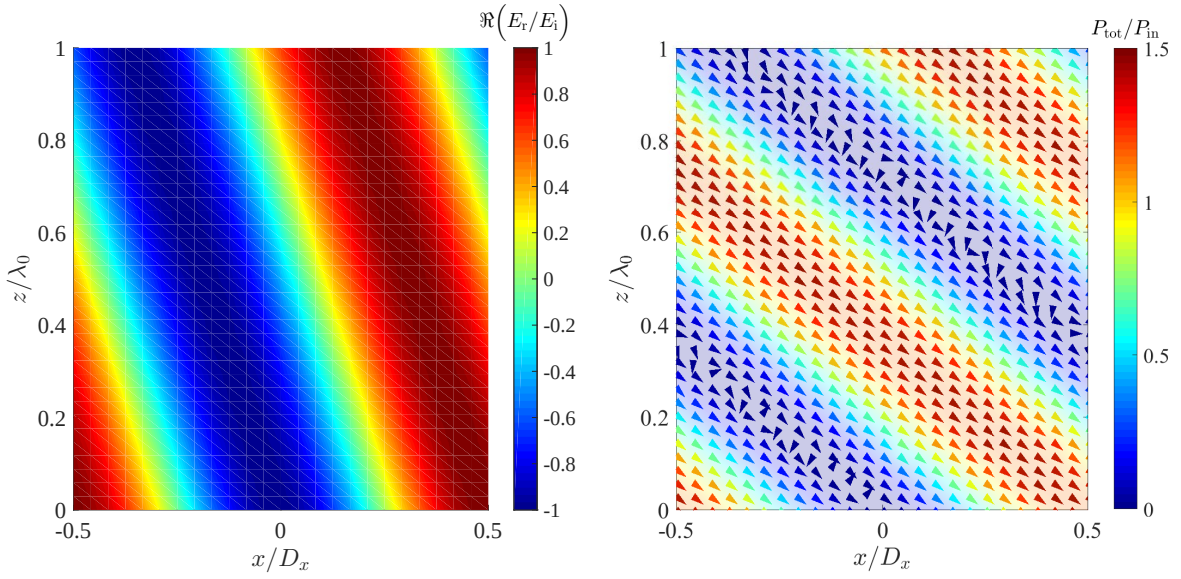

(a) (b)

FIG. 3: Lossy design of a reflector when $\theta_i = 0°$, $\theta_i = 70°$, $E_i = 1$ V/m and $f = 8$ GHz. (a) Real part of the scattered electric field. (b) Total power density distribution.

by considering the following tangential components of the electric and magnetic (for TE-polarized waves) fields:

$$E_{\rm t}(x,z) = E_{\rm i}\left(e^{-jk_1\sin\theta_{\rm i}x}e^{jk_1\cos\theta_{\rm i}z} + e^{-jk_1\sin\theta_{\rm r}x}e^{-jk_1\cos\theta_{\rm r}z}\right), \tag{6}$$

$$H_{\rm t}(x,z) = \frac{E_{\rm i}}{\eta_1}\left(\cos\theta_{\rm i}e^{-jk_1\sin\theta_{\rm i}x}e^{jk_1\cos\theta_{\rm i}z} - \cos\theta_{\rm r}e^{-jk_1\sin\theta_{\rm r}x}e^{-jk_1\cos\theta_{\rm r}z}\right). \tag{7}$$

The corresponding surface impedance, $Z_{\rm s}(x) = E_{\rm t}(x,0)/H_{\rm t}(x,0)$, reads

$$Z_{\rm s}(x) = \eta_1\frac{1+e^{j\Phi_{\rm r}(x)}}{\cos\theta_{\rm i} - \cos\theta_{\rm r}e^{j\Phi_{\rm r}(x)}}. \tag{8}$$

The impedance given by Eq. (8) is a complex number with some positive real part and the same period as in the conventional design (4). The real part in the surface impedance represents losses in the metasurface. Figure 3 shows the results of numerical simulations of a metasurface defined by Eq. (8) when $\theta_{\rm i} = 0°$, $\theta_{\rm r} = 70°$, $f = 8$ GHz, and $E_{\rm i} = 1$ V/m. The real part of the scattered field is represented in Fig. 3(a). We can see that a perfect plane wave with the amplitude $E_{\rm r} = 1$ V/m is reflected into the desired direction.

The real part of the Poynting vector is represented in Fig. 3(b), where we can see the power entering into the metasurface due to non-zero values of the real part of the impedance (the metasurface is lossy). The efficiency of this metasurface is $\eta = P_{\rm r}/P_{\rm i} = 0.34$ and the absorption is $A = 1 - P_{\rm r}/P_{\rm i} = 0.66$. Figure 3(b) shows that the magnitude of the power is modulated in the x-z plane with a flat wavefront. From the comparison between the spatial distributions of the electric field and the Poynting vector, it is easy to see that the tilt angle defining this modulation, $\theta_{\rm power}$, is different from the direction of the reflected wave phase front, $\theta_{\rm r}$. The Poynting vector can be expressed as:

$$P(x,z) = \frac{1}{2}{\rm Re}\{E_{\rm t}(x,z)H_z(x,z)^*\}\hat{x} - \frac{1}{2}{\rm Re}\{E_{\rm t}(x,z)H_{\rm t}(x,z)^*\}\hat{z}, \tag{9}$$

where the z-component of the magnetic field reads

$$H_z(x,z) = \frac{E_{\rm i}}{\eta_1}\left(\sin\theta_{\rm i}e^{-jk_1\sin\theta_{\rm i}x}e^{jk_1\cos\theta_{\rm i}z} + \sin\theta_{\rm r}e^{-jk_1\sin\theta_{\rm r}x}e^{-jk_1\cos\theta_{\rm r}z}\right). \tag{10}$$

The magnitude of the power flow vector can be found as $|P(x,z)| = \sqrt{P_x(x,z)^2 + P_z(x,z)^2}$, with $P_x(x,z)$ and $P_z(x,z)$ being the x-component and the z-component of the Poynting vector. The angle of the modulation can be easily found as

$$\sin\theta_{\rm power} = \frac{\partial|P(x,z)|/\partial x}{\partial|P(x,z)|/\partial z} = \frac{\sin\theta_{\rm r} - \sin\theta_{\rm i}}{\cos\theta_{\rm r} + \cos\theta_{\rm i}}. \tag{11}$$

In the scenario described in Figure 3, when $\theta_{\rm i} = 0°$ and $\theta_r = 70°$, the angle of the power modulation is $\theta_{\rm power} = 44.5°$. It is important to notice that in the conventional design described by Eq. 4, this modulation with a flat wave front in $\theta_{\rm power} = 44.5°$ also appears. However, the energy scattered in other directions significantly perturbs it.

C. "Active-lossy" design

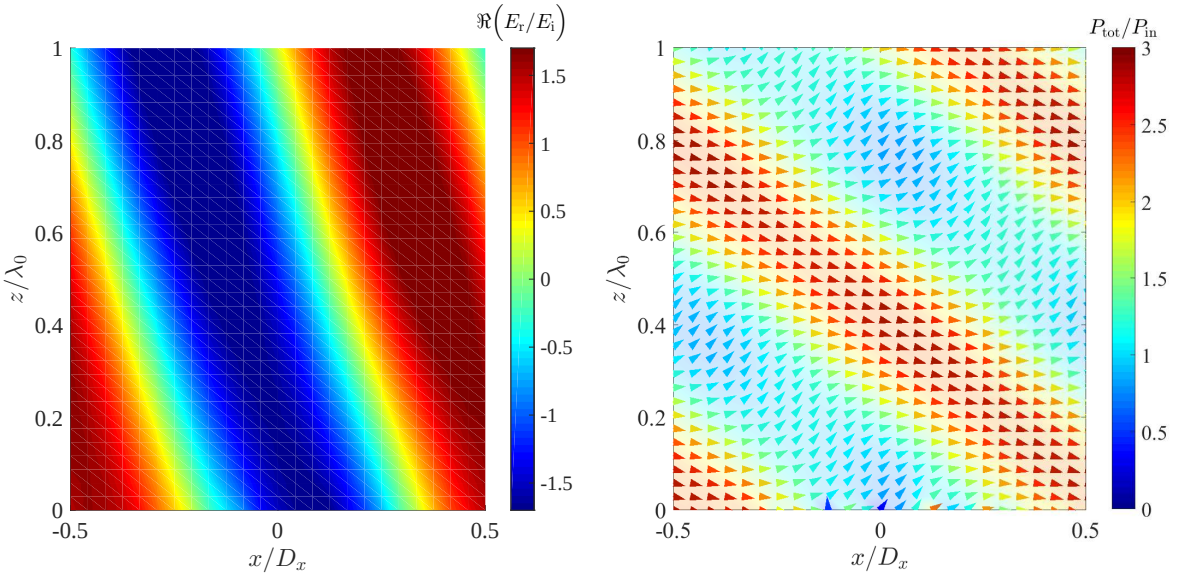

(a) (b)

FIG. 4: "Active-lossy" design of a reflector when $\theta_i = 0°$, $\theta_r = 70°$, $E_{\rm i} = 1$ V/m and $f = 8$ GHz. (a) Real part of the scattered electric field. (b) Total power density distribution.

In order to achieve perfect anomalous reflection, the power carried in the desired direction must be equal to the power of the incident plane wave, so the amplitude of the reflected wave has to be $E_{\rm r} = E_{\rm i}\frac{\sqrt{\cos\theta_{\rm i}}}{\sqrt{\cos\theta_{\rm r}}}$ [14]. Considering this condition, the tangential components of the electric and magnetic fields of the two plane waves (incident and reflected) at $z = 0$ are defined as

$$E_{\rm t}(x,z) = E_{\rm i}\left(e^{-jk_1\sin\theta_{\rm i}x}e^{jk_1\cos\theta_{\rm i}z} + E_{\rm r}e^{-jk_1\sin\theta_{\rm r}x}e^{-jk_1\cos\theta_{\rm r}z}\right), \quad (12)$$

$$H_{\rm t}(x,z) = \frac{1}{\eta_1}\left(E_{\rm i}\cos\theta_{\rm i}e^{-jk_1\sin\theta_{\rm i}x}e^{jk_1\cos\theta_{\rm i}z} - E_{\rm r}\cos\theta_{\rm r}e^{-jk_1\sin\theta_{\rm r}x}e^{-jk_1\cos\theta_{\rm r}z}\right), \quad (13)$$

which corresponds to the input impedance $Z_{\rm s}(x) = E_{\rm t}(x,0)/H_{\rm t}(x,0)$

$$Z_{\rm s}(x) = \frac{\eta_1}{\sqrt{\cos\theta_{\rm i}\cos\theta_{\rm r}}} \frac{\sqrt{\cos\theta_{\rm r}} + \sqrt{\cos\theta_{\rm i}}\, e^{j\Phi_{\rm r}(x)}}{\sqrt{\cos\theta_{\rm i}} - \sqrt{\cos\theta_{\rm r}}\, e^{j\Phi_{\rm r}(x)}}. \tag{14}$$

The analysis of this expression shows that the input impedance is a complex number, whose real part is a periodical function of x with the period dictated by Eq. (5). The real part of the input impedance periodically takes positive (corresponding to loss) and negative (gain) values. The power which passes through the input surface in the "lossy" regions is re-radiated from the "active" regions so that the overall metasurface response is lossless. Figure 4 shows numerical simulations for this design when $\theta_{\rm i} = 0°$, $\theta_{\rm r} = 70°$, $f = 8$ GHz and $E_{\rm i} = 1$ V/m. The real part of the scattered electric field is represented in Fig. 4(a). In this case, the scattered field corresponds to a plane wave with amplitude $E_{\rm r} = 1.7$ V/m, fulfilling the condition for the power conservation previously mentioned, and the power efficiency equals 100%. Figure 4(b) shows the power flow where one can visualize this behaviour. Thus, as was discussed in [14], passive metasurfaces with ideal anomalous reflection should behave as non-local antennas, receiving power in the "lossy" areas, and transmitting and re-radiating the same power in the "active" areas. As it was shown for the "lossy" case, the modulation in the magnitude of the power can be described by Eq. (11), so the direction of the modulation is $\theta_{\rm power} = 44.5°$.

Table I summarizes the field amplitudes and the power sent into the three directions ($\theta_{\rm i}$, $\theta_{\rm r}$, $-\theta_{\rm r}$) when the metasurface is illuminated by a normally incident plane wave with the amplitude $E_{\rm i} = 1$ V/m. It is clear that the "active-lossy" design promises perfect performance but its actual realization requires either the use of active (gain) elements or creation of carefully engineered non-local metasurfaces. In the rest of this paper we explain how such non-local surfaces can be realized and present the corresponding results. The last two rows in the table show the theoretical and experimental performance of these non-local perfect anomalous reflectors.

D. The concept of modulated leaky-wave surfaces

We think that probably the most reasonable approach to practical realization of perfectly reflecting lossless reflectors is to use inhomogeneous leaky-wave surfaces, generalizing the concept of leaky-wave antennas. Indeed, leaky-wave antennas are formed by perturbed

	θ_i	θ_r	$-\theta_\mathrm{r}$	Absorption	Efficiency
Generalized reflection law. Equation (4)	0.27/ 0.07	1.5/ 0.757	0.77/ 0.2	0	75.7 %
Lossy design dictated by Equation (8)	0/0	1/0.34	0/0	0.66	34 %
"Active-lossy" design dictated by Equation (14)	0/0	1.7/ 1	0/0	0	100%
Inhomogeneous leaky-wave antennas introduced in this paper.	0/0	1.7/ 1	0/0	0	100%
Implementation with metal patches (lossy materials)	0/0	1.66/0.94	0/0	0.06	94%

TABLE I: Numerical results and comparison between the different design possibilities for reflectarrrays. Amplitude/power of waves sent into the respective directions, absorption coefficient and power efficiency.

waveguides or transmission lines, naturally offering the needed channel for transporting power from receiving areas to transmitting areas. Even more importantly, tuning the inhomogeneity profiles along the antenna surface it appears possible to realize regimes where the receiving areas receive power predominantly from the illumination direction while the radiating areas send the waves predominantly in the desired direction of anomalous reflection. Thus, tuning the phase synchronism of free-space waves and leaky waves on the surface we can realize directive power transfer along the surface without using any non-reciprocal elements.

We start the study considering the surface-impedance model of a leaky-wave structure. Within this model, lossless reflectors are described by a reactive surface impedance $Z_{\mathrm{s}0}$. In order to allow propagation of surface waves of the considered TE polarization along the surface, which we need in order to realize the non-local reflection, we demand that the reactance is negative (capacitive) at every point of the surface. The tangential wavenumber

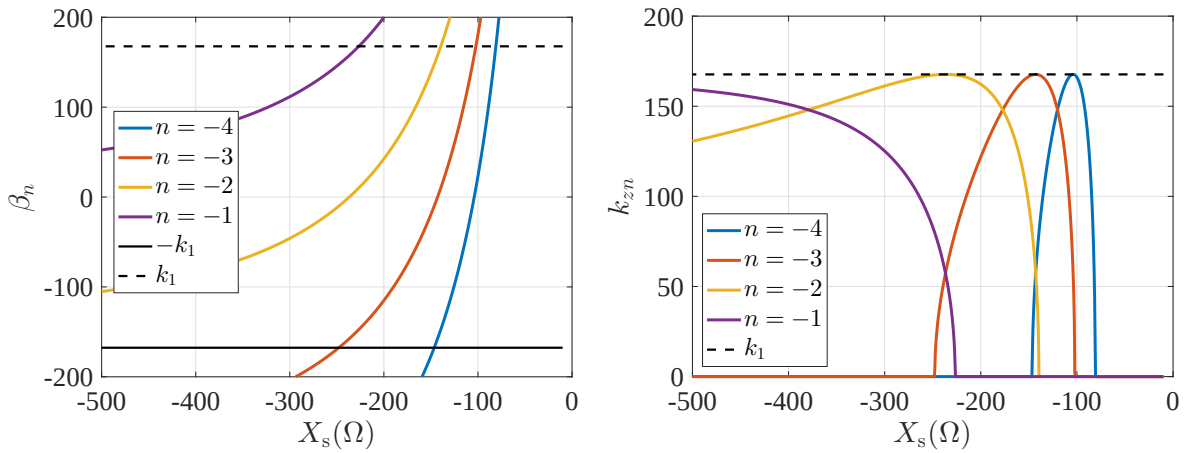

(a) (b)

FIG. 5: Tangential (a) and vertical (b) wavenumbers introduced in system due to a periodic perturbation with period $D_x = \lambda/|\sin\theta_i - \sin\theta_r|$ as a function of the surface impedance $Z_s = jX_s$

of the surface wave can be found using the relation

$$\beta_s = k_1\sqrt{\left(1 - \frac{\eta_1^2}{Z_{s0}^2}\right)}. \tag{15}$$

In order to couple the surface wave to free space, the reactance should be non-uniform over the reflector surface. In conventional leaky-wave antennas, where the goal is to launch a wave in a specific direction, the surface is periodically perturbed. This perturbation generates spatial harmonics whose tangential wave number can be expressed as

$$\beta_n = \beta_s + n\frac{2\pi}{D_x}, \tag{16}$$

where $n = \pm1, \pm2....$ The corresponding vertical wavenumbers, k_{zn}, can be found using

$$k_{zn} = \sqrt{{k_1}^2 - {\beta_n}^2}. \tag{17}$$

Knowing the vertical and tangential wavenumbers, the direction of the propagating waves is calculated using

$$\sin\theta_n = \frac{\beta_n}{k_1} = \sqrt{\left(1 - \frac{\eta_1^2}{Z_{s0}^2}\right)} + n\sin\theta_r. \tag{18}$$

Figures 5(a) and 5(b) represent the tangential and vertical wavenumbers for different values of the surface impedance $Z_{s0} = jX_{s0}$.

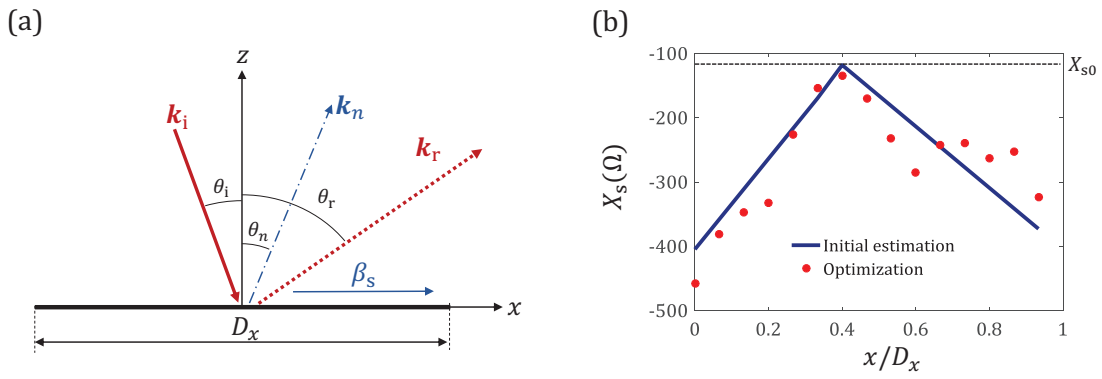

FIG. 6: (a) Schematic representation of the proposed design methodology for the perfect reflecting metasurface based on the leaky wave antenna behaviour with a modulation in the impedance profile. (b) Surface impedance of the metasurface when $\theta_r = 70°$ and $\theta_i = 0°$. Blue line represents the initial estimation of the surface reactance (Eq. (22)) and red dots represent the optimized values of the surface reactance on the discretized surface.

The impedance surface should be chosen in order to couple the energy to free space through leaky waves. For example, if we choose $X_{s0} = -124\ \Omega$, only the harmonics $n = -3$ and $n = -4$ propagate in free space. Particularly, for $X_{s0} = -124\ \Omega$ the waves propagate in the directions specified by $\theta_{-3} = 22.3°$ and $\theta_{-4} = -34°$. Once we have determined the surface impedance that allows surface-wave propagation and coupling with free-space waves, the reactance should be modulated. Conventional periodical modulations (usually with a sinusoidal profile) provide coupling to the waves along these two directions (in this example). But as we saw above, to realize perfect anomalous reflection, in the areas where the surface should receive power from the incident field, the wave along the surface should be in phase synchronism with the incident plane wave. In contrast, in the areas where the energy should be launched into the desired direction, the sync should hold for the reflected plane wave.

To realize such operation, we propose to modulate the reflection phase linearly, using the generalized reflection law separately for these two parts of the metasurface period. The required derivative of the local phase can be estimated by considering the additional effective "momentum" along the surface, in analogy with the generalized law of reflection. The

required linear phase dependence can be written as

$$\Phi_{\mathrm{r}}(x) = \begin{cases} (\sin\theta_{\mathrm{r}} - \sin\theta_n)k_1 x - \Phi_0 & 0 \le x < x_1 \\ (\sin\theta_{\mathrm{i}} - \sin\theta_n)k_1(x - D_x) - \Phi_0 & x_1 \le x < D_x. \end{cases} \tag{19}$$

In our particular example, the derivative has the opposite sign in the two parts of the surface period (shifting the angle $\theta_{-3} = 22.3^\circ$ to zero and 70°, respectively), and $x_1 = D_x \frac{\sin\theta_{\mathrm{n}} - \sin\theta_{\mathrm{i}}}{\sin\theta_{\mathrm{r}} - \sin\theta_{\mathrm{i}}}$ is the point where the derivative of the reflection phase changes from positive to negative. The initial phase shift reads

$$\Phi_0 = 2\pi \frac{(\sin\theta_{\mathrm{r}} - \sin\theta_n)(\sin\theta_n - \sin\theta_{\mathrm{i}})}{(\sin\theta_{\mathrm{r}} - \sin\theta_{\mathrm{i}})^2} - 2\arctan\frac{X_{\mathrm{s0}}}{\eta_1}. \tag{20}$$

Notice that $\Phi_{\mathrm{r}}(x_1) = 2\arctan\frac{X_{\mathrm{s0}}}{\eta_1}$ corresponds to the phase of the reflection coefficient for the homogeneous impedance surface with the surface impedance $Z_{\mathrm{s0}} = jX_{\mathrm{s0}}$. The relation between the phase gradient and the modulated surface impedance can be found through the reflection coefficient

$$\Phi_{\mathrm{r}}(x) = 2\arctan\frac{X_{\mathrm{s}}(x)}{\eta_1} \approx 2\frac{X_{\mathrm{s}}(x)}{\eta_1}, \tag{21}$$

where the approximation holds for small values of X_{s}/η_1. Using Eq. (21), we can estimate the modulations needed for the metasurface input impedance using the following expression:

$$X_{\mathrm{s}}(x) = \begin{cases} \frac{\eta_1}{2}(k_1(\sin\theta_{\mathrm{r}} - \sin\theta_{\mathrm{n}})x - \Phi_0) & 0 \le x < x_1 \\ \frac{\eta_1}{2}(k_1(\sin\theta_{\mathrm{i}} - \sin\theta_{\mathrm{n}})(x - D_x) - \Phi_0) & x_1 \le x < D_x. \end{cases} \tag{22}$$

The blue line in Fig. 6(b) represents the surface reactance profile defined by Eq. (22) when $X_{\mathrm{s0}} = -124\ \Omega$, $n = -3$, $\theta_{\mathrm{i}} = 0^\circ$, and $\theta_{\mathrm{r}} = 70^\circ$. Obviously, this analytical estimation of the perfect reactance profile is rather approximate, because we make use of the homogeneous reactance model in case when the assumption that the metasurface is uniform on the wavelength scale is not properly justified. For this reason next we do numerical optimization of the surface reactance, setting these estimations of the required reactance profile as the initial guess and using 15 elements for the discretization as a piece-wise homogeneous reactive impedance boundary. As a result, we find the profile shown in Fig. 6(b) with the red dots (one dot corresponds to one homogeneous reactive-surface element). As expected from the above theory, it is everywhere capacitive, growing in one half of the period and decaying inside the other half. The differences with the analytically predicted values are due to the approximations in the models and are caused mainly because of the periodic

conditions imposed over the unit cell and the piece-wise constant numerical model of the surface that force generation of more complex evanescent field structure than assumed in the analytical analysis.

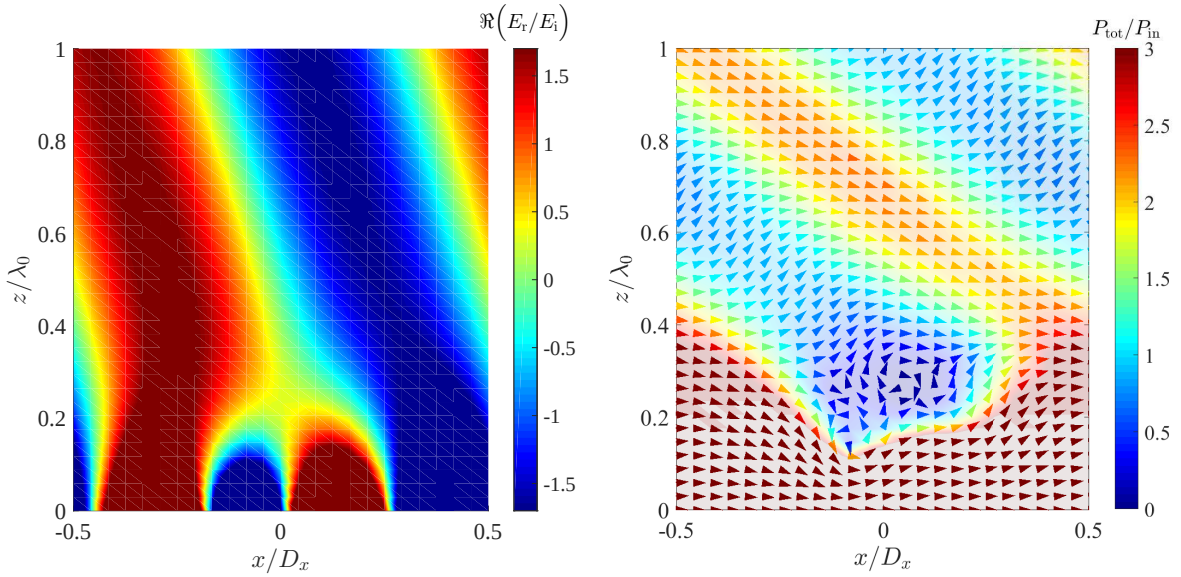

(a) (b)

FIG. 7: Lossless design of a perfect reflectarray based on the linearly-modulated leaky-wave antenna structure when $\theta_i = 0°$, $\theta_r = 70°$, $E_i = 1$ V/m and $f = 8$ GHz. (a) Real part of the scattered electric field. (b) Total power density flow distribution.

Numerical simulations of the corresponding field and the Poynting vector distributions are shown in Fig. 7. We clearly see that a surface wave propagating along the surface is indeed formed. If we now define a reference plane above the volume filled by the surface-mode fields (which is our "input port" to the metasurface structure) and look at the input impedance there, we see that it indeed satisfies the requirements of perfect operation: it is a complex value given by Eq. (14), and the real part is properly varying, emulating "loss" where the power is received by the leaky-wave structure and "gain" in the areas where it is launched back.

III. IMPLEMENTATION: INHOMOGENEOUS LEAKY-WAVE SURFACE

Previous results show the capability of surface waves propagating along an engineered gradient-phase metasurface to redirect energy and emulate the ideal "active-passive" be-

haviour needed for the implementation of perfect reflectarrays. As a particular realization of the required inhomogeneous leaky-wave surface we consider one of the simplest reactive impedance surfaces: a subwavelength array of metallic patches above a metal ground plane. If the array is periodical, the structure can be modelled as a uniform impedance surface, which supports TE surface waves if the dimensions are chosen so that the surface impedance is capacitive. A schematic representation of the proposed system is shown in Fig. 8(b).

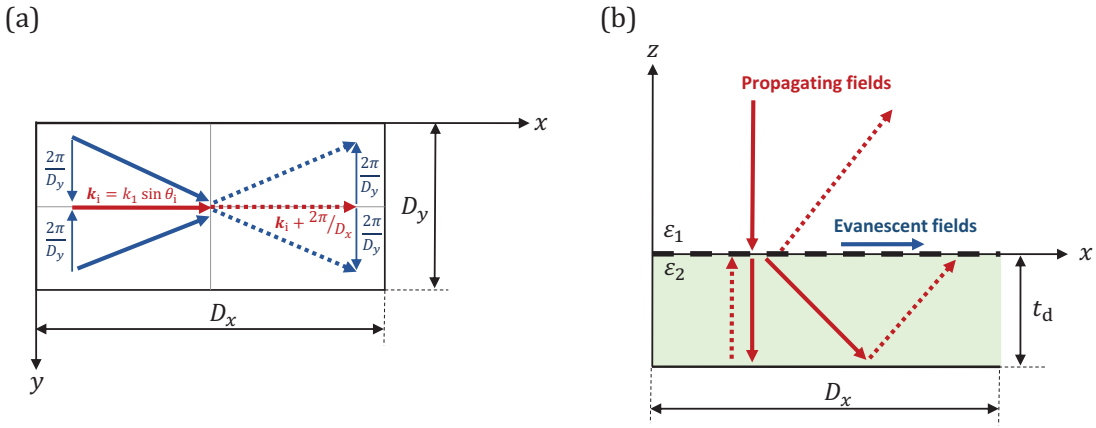

FIG. 8: Illustration of the desired performance of an ideally reflecting metasurface. TE incidence is assumed and the metasurface is located in the yz-plane.

In this scenario, we will extend the above analysis by including 2D periodicity in such a way that the evanescent waves can have a non-zero propagation constant along any direction contained in the metasurface plane. Invoking evanescent waves produced by 2D gratings, it is easer to satisfy the periodic conditions imposed at the boundaries of the unit cells by the incident plane wave.

The tangential component of the electric fields in the background medium (denoted by 'b') and in the substrate (denoted by 's') can be expressed as a superposition of propagating and evanescent fields:

$$E_t^{\mathrm{b,s}} = E_{\mathrm{pr}}^{\mathrm{b,s}} + E_{\mathrm{ev}}^{\mathrm{b,s}}. \tag{23}$$

Propagating fields in the background are the superposition of the incident plane wave with the amplitude E_{i} and the anomalously reflected plane wave with the amplitude $E_{\mathrm{r}} = E_{\mathrm{i}}\sqrt{\frac{\cos\theta_{\mathrm{i}}}{\cos\theta_{\mathrm{r}}}}$:

$$E_{\mathrm{pr}}^{\mathrm{b}} = E_{\mathrm{i}} e^{-jk_1 \sin\theta_{\mathrm{i}} x} e^{jk_1 \cos\theta_{\mathrm{i}} z} + E_{\mathrm{r}} e^{-jk_1 \sin\theta_{\mathrm{r}} x} e^{-jk_1 \cos\theta_{\mathrm{r}} z}. \tag{24}$$

In the substrate, the propagating waves are defined by

$$E_{\mathrm{pr}}^{\mathrm{s}} = A_1 e^{-jk_1 \sin\theta_{\mathrm{i}} x}(e^{jk_{z1}z} + R_1 e^{-jk_{z1}z}) + A_2 e^{-jk_1 \sin\theta_{\mathrm{r}} x}(e^{jk_{z2}z} + R_2 e^{-jk_{z2}z}), \tag{25}$$

where $k_{z1} = k_1\sqrt{\varepsilon_2 - \sin\theta_{\mathrm{i}}{}^2}$ and $k_{z2} = k_1\sqrt{\varepsilon_2 - \sin\theta_{\mathrm{r}}{}^2}$ are the vertical wavenumbers of the propagating waves, $R_1 = -e^{-2jk_{z1}t_{\mathrm{d}}}$ and $R_2 = -e^{-2jk_{z2}t_{\mathrm{d}}}$ are the reflection coefficients from the ground plane and t_{d} is the thickness of the dielectric. The tangential component of the evanescent fields in the background are expressed as

$$E_{\mathrm{ev}}^{\mathrm{b}} = B_1 e^{-jk_1 \sin\theta_{\mathrm{i}} x} e^{-\alpha_1 z} \cos\left(\frac{2\pi}{D_{\mathrm{y}}} y\right) + B_2 e^{-jk_1 \sin\theta_{\mathrm{r}} x} e^{-\alpha_2 z} \cos\left(\frac{2\pi}{D_{\mathrm{y}}} y\right), \tag{26}$$

where $\alpha_1 = \sqrt{k_1^2 \sin\theta_{\mathrm{i}}{}^2 + \left(\frac{2\pi}{D_{\mathrm{y}}}\right)^2 - k_1^2}$ and $\alpha_2 = \sqrt{k_1^2 \sin\theta_{\mathrm{r}}{}^2 + \left(\frac{2\pi}{D_{\mathrm{y}}}\right)^2 - k_1^2}$ are the attenuation constants of the evanescent field. Evanescent fields in the substrate must have the same tangential wave vector as the evanescent field above the interface:

$$E_{\mathrm{ev}}^{\mathrm{s}} = B_3 e^{-jk_1 \sin\theta_{\mathrm{i}} x}(e^{\alpha_3 z} + R_3 e^{-\alpha_3 z}) \cos\left(\frac{2\pi}{D_{\mathrm{y}}} y\right) + B_4 e^{-jk_1 \sin\theta_{\mathrm{r}} x}(e^{\alpha_4 z} + R_4 e^{-\alpha_4 z}) \cos\left(\frac{2\pi}{D_{\mathrm{y}}} y\right), \tag{27}$$

where $\alpha_3 = \sqrt{k_1^2 \sin\theta_{\mathrm{i}}{}^2 + \left(\frac{2\pi}{D_{\mathrm{y}}}\right)^2 - k_1^2\varepsilon_2}$ and $\alpha_4 = \sqrt{k_1^2 \sin\theta_{\mathrm{r}}{}^2 + \left(\frac{2\pi}{D_{\mathrm{y}}}\right)^2 - k_1^2\varepsilon_2}$ are the attenuation constants of the evanescent fields in the substrate, and $R_3 = -e^{-2\alpha_3 t_{\mathrm{d}}}$ and $R_4 = -e^{-2\alpha_4 t_{\mathrm{d}}}$ are the reflection coefficients of the evanescent fields from the ground plane. Imposing the countinuity of the tangential fields at $z = 0$ we can find the amplitudes of the waves

$$A_1 = \frac{E_{\mathrm{i}}}{1 + R_1}, \qquad A_2 = \frac{E_{\mathrm{r}}}{1 + R_2}, \tag{28}$$

$$B_3 = \frac{B_1}{1 + R_3}, \qquad B_4 = \frac{B_2}{1 + R_4}. \tag{29}$$

The patches are aligned with the center at $y = 0$, which forces zero tangential electric field at $y = 0$. We can find the amplitudes of the waves just defining $B_1 = -E_{\mathrm{i}}$ and $B_2 = -E_{\mathrm{r}}$. Figure 9(a) shows the real part of the electric field distribution in the xz-plane at $y = 0$. In the bottom panel, Fig. 9(c) shows the real part of the electric field distribution in the xy-plane at $z = 0$. It is important to notice that at $y = \pm D_y/4$ the effect of the evanescent fields vanishes and the electric and magnetic fields above the metasurface are identical to the ones described by Eq. (12), i.e., the input impedance is described by Eq. (14).

The modulation of the field is done by changing the length of the patches. Our design contains 10 patches per unit cell, all of them with the same width $w = 3.5$ mm and centred

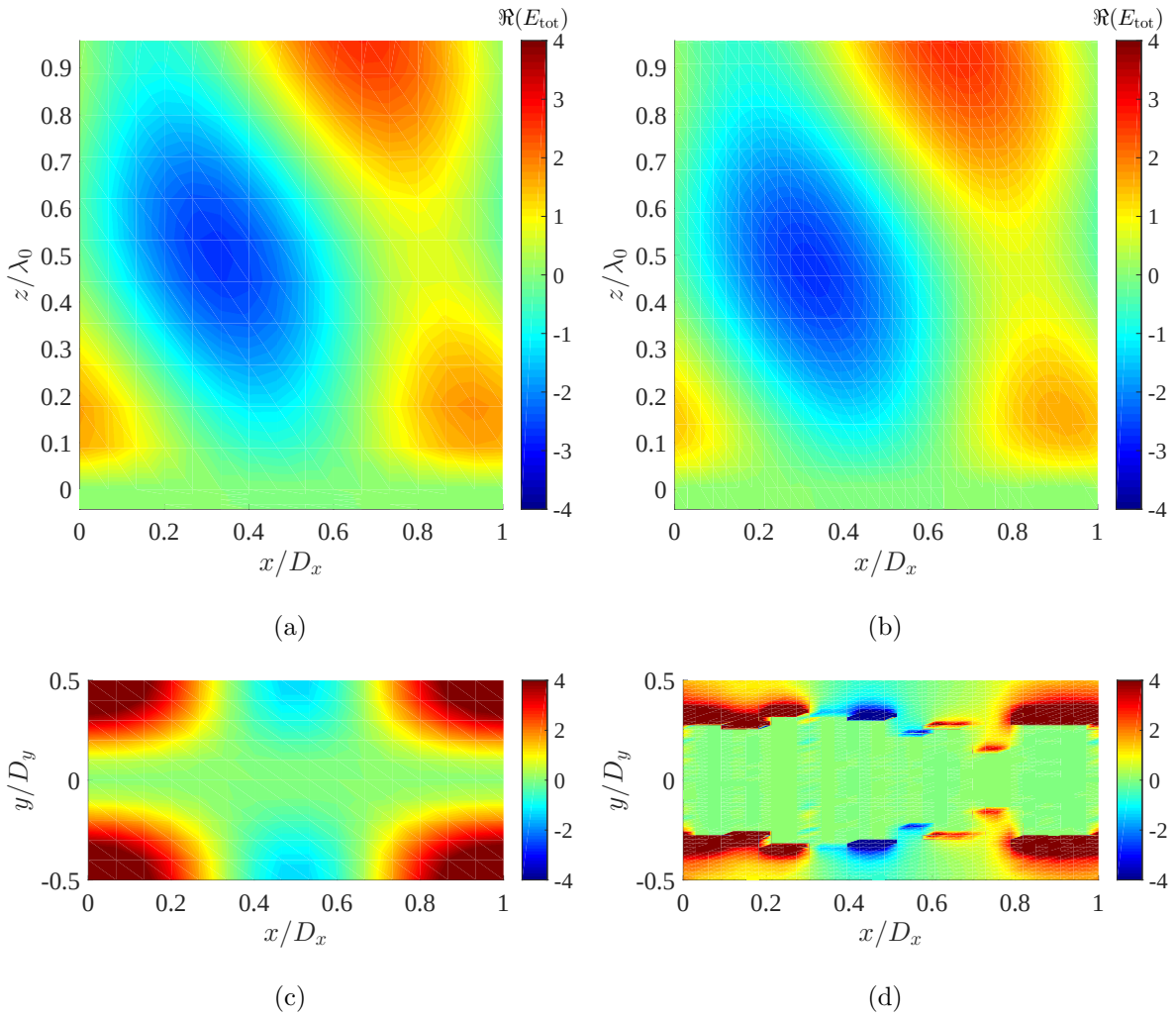

FIG. 9: Real part of the total electric field. (a) and (b) represent the theoretical and simulated field distributions on the xz-plane when $y = 0$. (c) and (d) represent the theoretical and simulated field distributions on the xy-plane when $z = 0$.

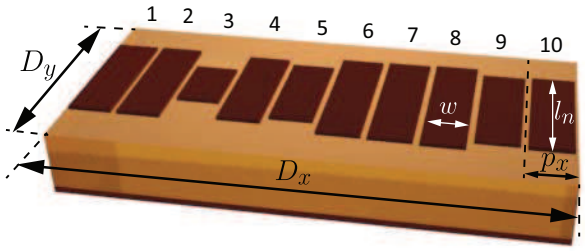

FIG. 10: Schematic representation of one unit cell.

along the $y = 0$ line. A schematic representation of the proposed structure is illustrated

$l_1 = 10.7$ mm	$l_2 = 10.3$ mm	$l_3 = 12.3$ mm	$l_4 = 12$ mm	$l_5 = 11.8$ mm	$l_6 = 8.7$ mm	$l_7 = 10.2$ mm
$l_8 = 5.4$ mm	$l_9 = 11$ mm	$l_{10} = 10.9$ mm	$t_d = 1.575$ mm	$w = 3.5$ mm	$D_x = 40$ mm	$D_y = 18.75$ mm

TABLE II: Physical dimensions of one unit cell.

by Fig. 10. For designing the array of patches which produces proper coupling with the evanescent modes, first we determine the required reflected field for each element. To do that, we use the phase gradient defined by Eq. (14). Then we periodically arrange each element (using a homogeneous array model) and calculate the length that produces the desired phase shift. Once we know the dimensions of all the elements in the unit cells we do a numerical optimization of the structure that corrects the effects produced in the non-homogeneous array that are not considered in the initial locally homogeneous approximation. The final dimensions of our design are summarized in Table II. For comparison with the theoretical model, Figs. 9(b) and (d) show the electric field distribution of the metasurface with 10 patches per unit cell.

Figure 11(b) shows the simulated total Poynting vector distributions in the xz-plane when $y = D_y/2$. The Poynting vector is distributed according to our predictions, the power is guided below the patches and then it is launched into the desired direction. The power distribution in the plane which contains the patches is shown in Fig. 11(c). We can see how the power is guided along the edges of the patches.

IV. EXPERIMENTAL REALIZATION AND CHARACTERIZATION

The metasurface sample designed to operate at the frequency 8 GHz was manufactured using conventional printed circuit board technology on a 1.575 mm thick Rogers 5880 substrate ($\epsilon_{\rm r} = 2.2$, $\tan\delta = 0.0009$). The sample comprised 11 unit cells along the x-axis and 14 unit cells along the y-axis [see Fig. 12(a)] and has size of $11.7\lambda = 440$ mm and $7\lambda = 262.5$ mm, respectively.

The operation of the proposed reflecting metasurface was verified by the measurements in an anechoic chamber emulating free-space environment. A vector network analyzer was connected to a transmitting quad-ridged horn antenna with 11 dBi gain at 8 GHz [see Fig. 12(b)]. The metasurface was located at a distance of 5.5 m (about 147λ) from the

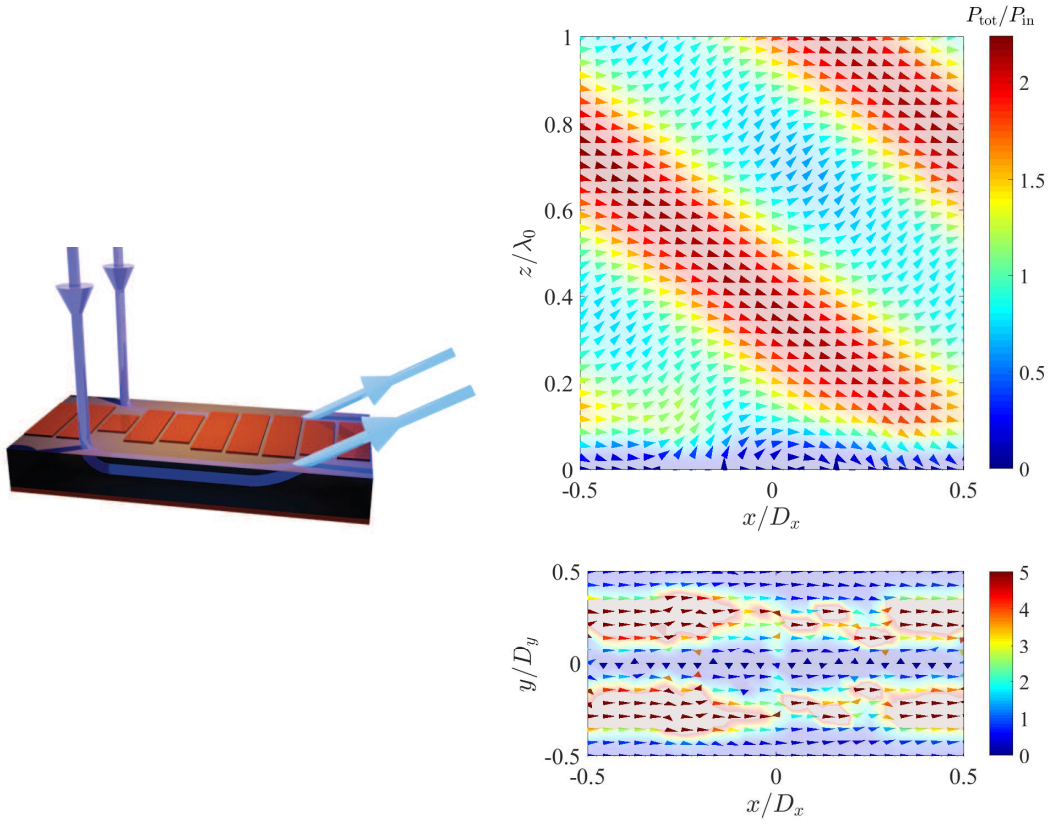

FIG. 11: Schematic representation of energy channelling in the metasurface (left). Real part of the total Poynting vector in the xz-plane when $y = D_y/2$ and real part of the Poynting vector in the xy-plane when $z = 0$.

transmitting antenna where the radiation from the antenna can be approximated as a plane wave. To control the metasurface orientation, it was attached to a platform rotating around the y-axis. The receiving antenna, identical to the transmitting one, was positioned at a distance 2.387 m (about 64λ) from the center of the metasurface. Both antennas and the metasurface form in space a triangle with an angle 70° at the metasurface center.

In the first experiment, the platform with the metasurface was rotating at an angle ϕ, while the positions of the antennas were fixed. Angle ϕ was counted from the line connecting the metasurface center and the transmitting antenna towards the normal to the metasurface plane (positive ϕ corresponded to the clockwise rotation of the platform when seen from the top). The signal reflected from the metasurface and measured by the receiving antenna $|S_{21,\mathrm{m}}|$ for different angles ϕ is shown in Fig. 13(a). The experimental data was measured at the resonance of the metasurface occurring at 8.08 GHz. The main peak of reflection

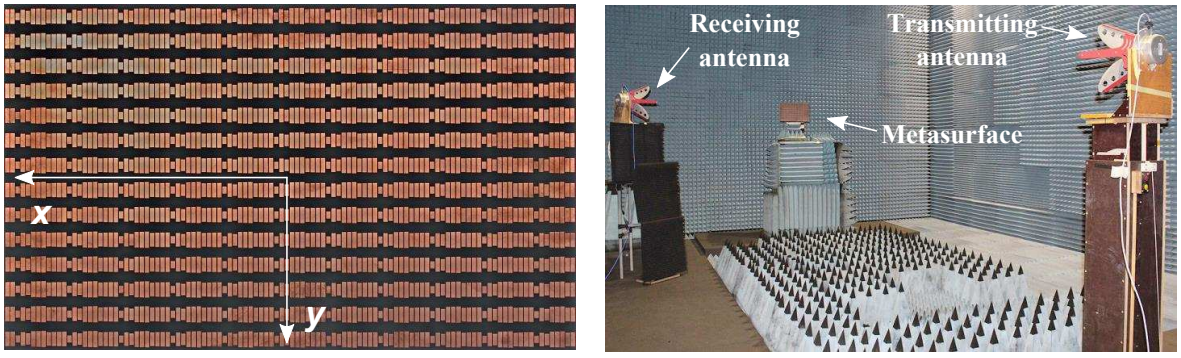

(a) (b)

FIG. 12: (a) Fabricated metasurface. (b) Experimental set-up in an anechoic chamber.

towards the receiving antenna occurs when the metasurface is illuminated normally. This is an expected result meaning that in this case most of the power impinging on the surface is reflected at 70° from the normal. The second peak occurring when $\phi = 35°$ corresponds to the specular reflection (incidence and reflection angles are equal) from the metamirror. This small non-zero specular reflections are acceptable because the metamirror was designed to have zero specular reflections only when illuminated normally.

In order to estimate the reflection efficiency of the metasurface ξ_{r}, in the second experiment we replaced the metasurface by an aluminium plate of the same size. The corresponding signal reflected from the plate and measured by the receiving antenna $|S_{21,\mathrm{p}}|$ versus angle ϕ is shown in Fig. 13(b). Now the single peak of reflection occurs when the plate is illuminated at 35°, which corresponds to the specular reflection. To find the reflection efficiency of the metasurface, we normalize its signal amplitude $|S_{21,\mathrm{m}}|$ for $\phi = 0°$ by the signal amplitude from the reference uniform metal mirror $|S_{21,\mathrm{p}}|$ for $\phi = 35°$. We additionally divide the obtained value by the correction factor $\xi_0 = |S_{21,0\mathrm{m}}|/|S_{21,0\mathrm{p}}|$ which gives the ratio between the theoretically calculated signal amplitudes from an *ideal* metasurface (of the same size and made of lossless materials) and a perfect conductor plate. The correction factor ξ_0 is less than unity because in this scenario the radiating effective area of the perfect conductor plate is greater than that of the ideal reflecting metasurface due to a different orientation with respect to the antennas. At the frequency 8.08 GHz in our particular configuration, the correction factor is equal to $\xi_0 = -2.41$ dB [17]. Thus, the reflection efficiency of the

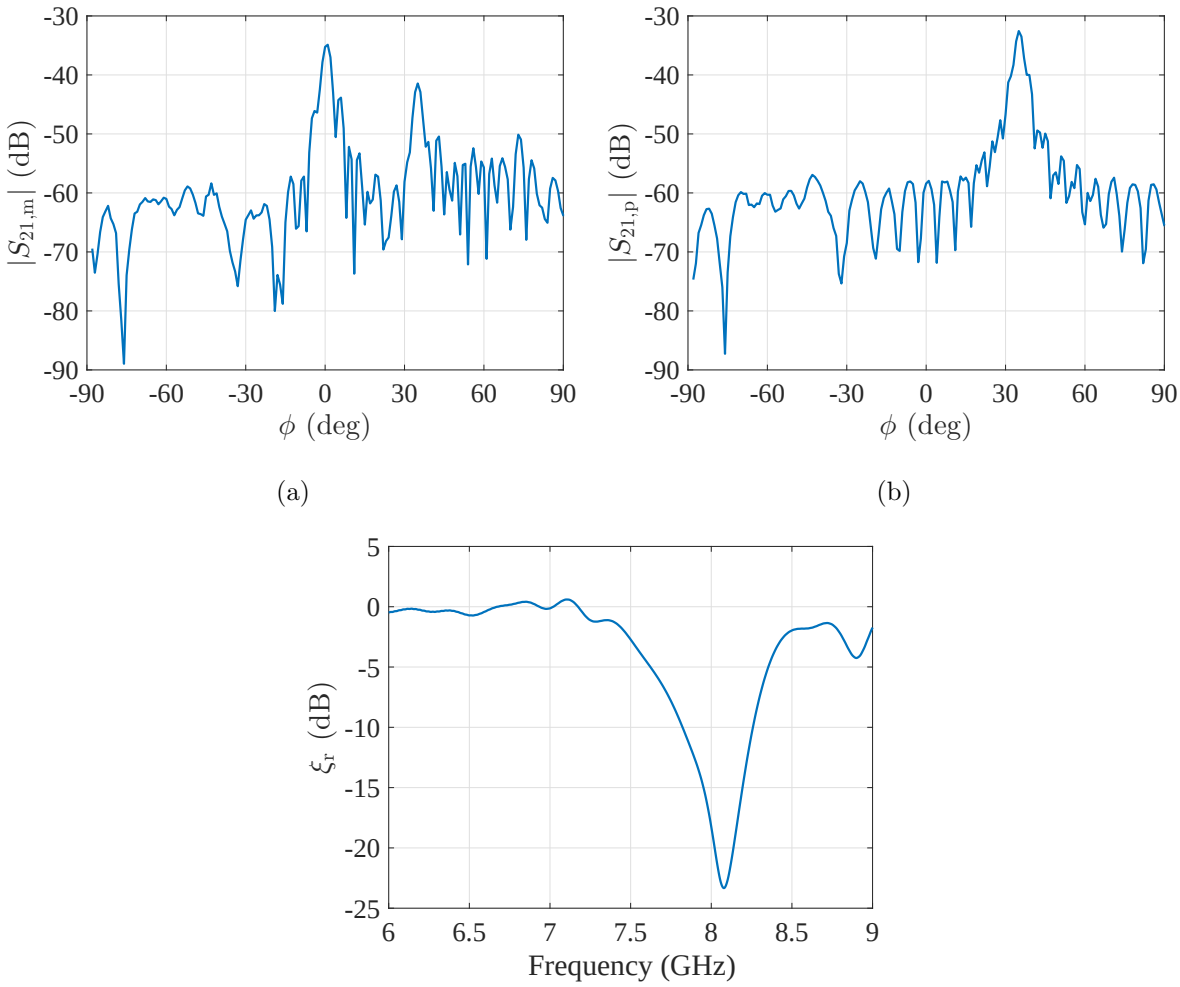

FIG. 13: Signals measured by the receiving antenna for different orientation angles ϕ of (a) the metasurface and (b) the metal plate of equal size. (c) Reflection efficiency of the metasurface illuminated normally.

metasurface is calculated as

$$\xi_\mathrm{r} = \frac{1}{\xi_0}\frac{|S_{21,\mathrm{m}}(\phi = 0^\circ)|}{|S_{21,\mathrm{p}}(\phi = 35^\circ)|} = -0.28 \text{ dB}. \tag{30}$$

In the linear scale and expressed in terms of power, the reflection efficiency reaches 93.8%. This result is in excellent agreement with the efficiency 94% obtained using numerical solver (see Table I). The remaining 6.2% of power incident on the metasurface is mainly absorbed by it.

In the third measurement, we fixed the orientation of the metasurface at $\phi = 0^\circ$ and utilized the transmitting antenna (fixed at the same position as in previous measurements)

as both the transmitter and receiver. Using conventional time gating post-processing procedure, we could filter out all parasitic reflections received by the antenna (from the walls, absorbers, and due to the impedance mismatch between the antenna and the cables), retaining only the signal reflected from the metasurface. The measured signal amplitude was normalized by the corresponding amplitude from the reference uniform aluminium plate which was measured likewise. This ratio, plotted in Fig. 13(c), represents the level of specular reflection from the metasurface $\xi_{\rm r}$ when illuminated normally. As is seen, at the resonance frequency 8.08 GHz the specular reflection is $\xi_{\rm r} = -23.33$ dB, which corresponds to 0.5% of the incident power. This result additionally confirms that the normally illuminated metasurface reflects all the power at the desired angle 70°. As is seen from Fig. 13(c), at frequencies below 7.2 GHz where the metal strips on the substrate are weakly excited, the metasurface behaves as a usual mirror obeying the simple reflection law.

V. CONCLUSION

In conclusion, we have demonstrated that by proper design of planar inhomogeneous low-loss reflectors it is possible to realize conceptually perfect anomalous reflection, transforming a plane wave coming from an arbitrary direction into a single plane wave propagating into any other direction. The introduced approach fully removes the fundamental limitations on the performance of known reflectarray antennas and known metasurfaces designed with the use of the generalized Snell's law. The "active-lossy" behavior of conceptually perfect anomalously reflected metasurfaces was realized with the use of carefully engineered effects of strong spatial dispersion in an inhomogeneous leaky-wave structure. Although in this first demonstration we assumed that the incidence is a single plane wave, the proposed physical mechanism of non-local reflections allows generalizations for arbitrary illuminations, opening possibilities for creation of metasurfaces for shaping waves without loosing power for parasitic scattering. Simple topology of metal parches printed on a thin dielectric structure makes the proposed designs attractive in practical applications.

ACKNOWLEDGMENT

This work was supported in part by the Academy of Finland (project 287894).

---

[1] J. Huang and J. A. Encinar, *Reflectarray Antennas* (Wiley, New Jersey, 2008).

[2] D. Sievenpiper, L. Zhang, R. F. J. Broas, N. G. Alexópolous, and E. Yablonovitch, *High-Impedance Electromagnetic Surfaces with a Forbidden Frequency Band*, IEEE Trans. Microw. Theory Tech. 47, 2059 (1999).

[3] D.M. Pozar, *Wideband reflectarrays using artificial impedance surfaces*, Electron. Lett. 43, 148 (2007).

[4] S. B. Glybovski, S. A. Tretyakov, P. A. Belov, Y. S. Kivshar, and C. R. Simovski, *Metasurfaces: From microwaves to visible*, Physics Reports, http://dx.doi.org/10.1016/j.physrep.2016.04.004 (2016).

[5] N. Yu, P. Genevet, M. A. Kats, F. Aieta, J.-P. Tetienne, F. Capasso, and Z. Gaburro, *Light Propagation with Phase Discontinuities: Generalized Laws of Reflection and Refraction*, Science 334, 333 (2011).

[6] S. Sun, K.-Y. Yang, C.-M. Wang, T.-K. Juan, W. T. Chen, C. Y. Liao, Q. He, S. Xiao, W.-T. Kung, G.-Y. Guo, L. Zhou, and D. P. Tsai, *High-Efficiency Broadband Anomalous Reflection by Gradient Meta-Surfaces*, Nano Lett. 12, 6223 (2012).

[7] A. Pors, M. G. Nielsen, R. L. Eriksen, and S. I. Bozhevolnyi, *Broadband Focusing Flat Mirrors Based on Plasmonic Gradient Metasurfaces*, Nano Lett. 13, 829 (2013).

[8] A. Pors and S. I. Bozhevolnyi, *Plasmonic Metasurfaces for Efficient Phase Control in Reflection*, Opt. Express 21, 27438 (2013).

[9] M. Farmahini-Farahani and H. Mosallaei, *Birefringent Reflectarray Metasurface for Beam Engineering in Infrared*, Opt. Lett. 38, 462 (2013).

[10] M. Esfandyarpour, E. C. Garnett, Y. Cui, M. D. McGehee, and M. L. Brongersma, *Metamaterial Mirrors in Optoelectronic Devices*, Nat. Nanotechnol. 9, 542 (2014).

[11] M. Kim, A. M. H. Wong, and G. V. Eleftheriades, *Optical Huygens Metasurfaces with Independent Control of the Magnitude and Phase of the Local Reflection Coefficients*, Phys. Rev. X 4, 041042 (2014).

[12] M. Veysi, C. Guclu, O. Boyraz, and F. Capolino, *Thin Anisotropic Metasurfaces for Simultaneous Light Focusing and Polarization Manipulation*, Journ. Opt. Soc. Am. B 32, 2 (2015).

[13] Z. Li, E. Palacios, S. Butun, and K. Aydin, *Visible-Frequency Metasurfaces for Broadband Anomalous Reflection and High-Efficiency Spectrum Splitting*, Nano Letters 15, 3 (2015).

[14] V. S. Asadchy, M. Albooyeh, S. N. Tcvetkova, A. Díaz-Rubio, Y. Ra'di, and S. A. Tretyakov, *Perfect control of reflection and refraction using spatially dispersive metasurfaces*, Phys. Rev. B. 94, 075142 (2016).

[15] N. M. Estakhri and A. Alù, *Wavefront Transformation with Gradient Metasurfaces*, submitted manuscript, accepted in PRX.

[16] A. Epstein and G. V. Eleftheriades, *Synthesis of Passive Lossless Metasurfaces Using Auxiliary Fields for Reflectionless Beam Splitting and Perfect Reflection*, arxiv.org/1607.02954, 14.06.2016.

[17] See supplementary materials.

SUPPLEMENTARY MATERIALS

Appendix A: Scattered fields from a metal plate illuminated obliquely

In this paragraph we analytically estimate scattering properties of a reference metal plate illuminated by an incident wave at an angle ϕ. In particular, we are interested in the amplitude of the scattered wave in the specular direction, i.e. when the angles of incidence and reflection are equal. Geometry of the problem is shown in Fig. 14. The receiving antenna is located at a distance $R = 2.387$ m from the center of the plate. In addition to the Cartesian coordinate system xyz used in the main text, it is convenient to introduce a local coordinate system uyn, where coordinates u and y define the plate plane, and the axis n defines its normal (for clarity not shown in the figure). We define the dimensions of the plate along u and y axis as $a = 440$ mm and $b = 262.5$ mm, respectively.

Assuming that the incident wave from the transmitting antenna located at 147λ distance from the plate is planar, the electric current induced on the plate surface reads, in the physical optics approximation,

$$\mathbf{j}_{\mathrm{e}}(u) = \mathbf{y} E_0 \frac{2}{\eta_1} \cos\phi \cdot e^{jk_1 u \sin\phi}, \tag{A1}$$

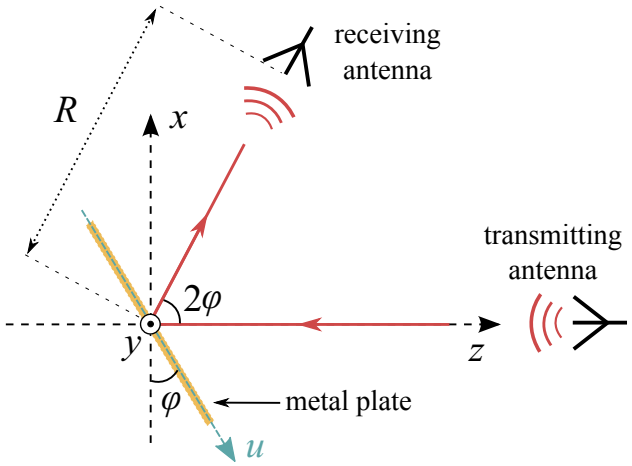

FIG. 14: Geometry of the problem with a metal plate.

where E_0 is the incident electric field at the center of the plate, eta_1 is the vacuum impedance, and k_1 is the wavenumber in free space. Here, the time-harmonic dependence in the form $e^{j\omega t}$ is assumed. After some calculations, the distance between a current element with the coordinates (u, y) and the receiving antenna can be written as

$$r(u,y) = \sqrt{u^2 + y^2 + 2uR\sin\phi + R^2}. \tag{A2}$$

Next, we calculate the electric vector potential $\mathbf{A}$ created by the currents given by (A1):

$$\mathbf{A} = \frac{1}{4\pi}\int\limits_S \mathbf{j}_{\mathrm{e}}(u)\frac{e^{-jk_1 r(u,y)}}{r(u,y)}\,\mathrm{d}S = \mathbf{y}\,\frac{E_0\cos\phi}{2\pi\eta_1}\int_{-a/2}^{a/2}\mathrm{d}u\int_{-b/2}^{b/2}\frac{e^{jk_1[u\sin\phi - r(u,y)]}}{r(u,y)}\,\mathrm{d}y, \tag{A3}$$

where $\mathrm{d}S = \mathrm{d}u\mathrm{d}y$ is the area element of the metal plate. The scattered electric field from the plate at the location of the receiving antenna reads

$$\mathbf{E}_{\mathrm{sc\,p}} = -j\omega\mu_0\mathbf{A} = -\mathbf{y}\,\frac{jk_1E_0\cos\phi}{2\pi}\int_{-a/2}^{a/2}\mathrm{d}u\int_{-b/2}^{b/2}\frac{e^{jk_1[u\sin\phi - r(u,y)]}}{r(u,y)}\,\mathrm{d}y. \tag{A4}$$

Appendix B: Scattered fields from the normally illuminated metasurface

In this paragraph we analytically estimate the scattering properties of the anomalously reflecting metasurface normally illuminated by an incident plane wave. In particular, we are interested in the amplitude of the scattered wave at an angle 70° from the normal. Geometry of the problem is shown in Fig. 15. The receiving antenna is located at the same distance $R = 2.387$ m from the center of the plate. In our analysis we use the idea that

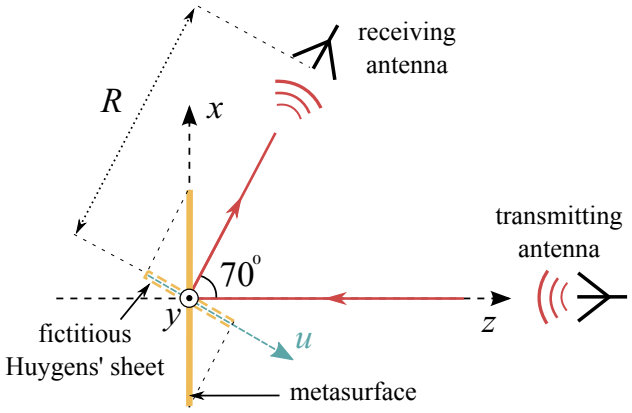

FIG. 15: Geometry of the problem with a metasurface.

an ideal reflecting metasurface has the same scattering properties as a fictitious sheet of Huygens' currents (electric and magnetic) oriented orthogonally to the main reflected beam (see Fig. 15). As is seen from the illustration, the dimensions of such a fictitious current sheet are $a\cos 70^\circ$ and b along the u and y axes, respectively. Thus, the area of the current sheet is smaller than that of the metasurface. This results in weaker scattering from the metasurface as compared with the metal plate of the same size.

To find the fictitious currents emulating the metasurface scattering, we need to know the reflected fields from the metasurface (under the assumption that the metasurface is infinite). As it was shown in the main text in Section IIC, these fields in our configuration read

$$\mathbf{E}_\mathrm{r} = \mathbf{y}\,\frac{E_0}{\sqrt{\cos 70^\circ}}, \qquad \mathbf{H}_\mathrm{r} = \mathbf{u}\,\frac{E_0}{\eta_1\sqrt{\cos 70^\circ}}. \tag{B1}$$

Next, we write the fictitious Huygens' currents which emulate the same reflected fields:

$$\mathbf{j}_\mathrm{e} = -\mathbf{y}\,\frac{E_0}{\eta_1\sqrt{\cos 70^\circ}}, \qquad \mathbf{j}_\mathrm{m} = -\mathbf{u}\,\frac{E_0}{\sqrt{\cos 70^\circ}}. \tag{B2}$$

Note that these currents are uniform and do not depend on the coordinates at the sheet. Next, we calculate the scattered fields from the electric currents. It could be shown that the scattered fields from the magnetic currents are identical. As is seen from Fig. 15, the distance between a current element with the coordinates (u, y) and the receiving antenna can be written as

$$r(u,y) = \sqrt{u^2 + y^2 + R^2}. \tag{B3}$$

Next, we calculate the electric vector potential $\mathbf{A}$ created by the electric currents:

$$\mathbf{A} = \frac{1}{4\pi}\int\limits_S \mathbf{j}_\mathrm{e}\frac{e^{-jk_1 r(u,y)}}{r(u,y)}\,\mathrm{d}S = -\mathbf{y}\,\frac{E_0}{4\pi\eta_1\cos 70^\circ}\int_{-a/2\cos 70^\circ}^{a/2\cos 70^\circ}\mathrm{d}u\int_{-b/2}^{b/2}\frac{e^{-jk_1 r(u,y)}}{r(u,y)}\,\mathrm{d}y. \tag{B4}$$

The scattered electric field from the metasurface at the location of the receiving antenna will be double of the field scattered by the electric currents at the sheet (the electric and magnetic currents have equal contributions):

$$\mathbf{E}_{\mathrm{sc\,m}} = \mathbf{y}\,\frac{jk_1E_0}{2\pi\cos 70^\circ}\int_{-a/2\cos 70^\circ}^{a/2\cos 70^\circ}\mathrm{d}u\int_{-b/2}^{b/2}\frac{e^{-jk_1r(u,y)}}{r(u,y)}\,\mathrm{d}y. \tag{B5}$$

Appendix C: Correction factor for the signal amplitudes measured in the experiment

The correction factor introduced in the main text represents the ratio between the theoretically calculated signal amplitudes from the ideal metasurface and a perfect conductor plate $\xi_0 = |S_{21,0\mathrm{m}}|/|S_{21,0\mathrm{p}}|$. Obviously, this ratio is equal to the ratio between the scattered electric fields in the two cases, i.e. $\xi_0 = |E_{\mathrm{sc\,m}}/E_{\mathrm{sc\,p}}|$. Using expressions (A4) and (B5) and assuming $\phi = 35^\circ$, we find that for our configuration $\xi_0 = 0.758 = -2.41$ dB. Interestingly, when the distance between the receiving antenna and the metasurface R tends to infinity, the correction factor can be calculated using a simple trigonometric formula: $\xi_0 = \sqrt{\cos 70^\circ}/\cos\phi$.